

New Perovskite Oxide $\text{CaCu}_3\text{Cr}_2\text{Ru}_2\text{O}_{12}$: Comparison with Structural, Magnetic, and Transport Properties of the $\text{CaCu}_3\text{B}_2\text{B}'_2\text{O}_{12}$ Perovskite Family

Song-Ho Byeon,^{*,†} Seoung-Soo Lee,[†] John B. Parise,^{*,‡} and Patrick M. Woodward[§]

College of Environment and Applied Chemistry, Kyung Hee University, Kyung Ki 449-701, Korea, Department of Geosciences and Chemistry Department, State University of New York, Stony Brook, New York 11794-2100, and The Ohio State University, Department of Chemistry, Columbus, Ohio 43210-1185

Received April 11, 2006. Revised Manuscript Received June 2, 2006

A new member of the $\text{CaCu}_3\text{B}_2\text{B}'_2\text{O}_{12}$ perovskite family, $\text{CaCu}_3\text{Cr}_2\text{Ru}_2\text{O}_{12}$, has been synthesized at 12 GPa and 1150 °C. Rietveld refinement using powder X-ray diffraction data reveals that this oxide crystallizes in space group $Im\bar{3}$ where cations are disordered over the octahedral B site. Measurements of magnetic susceptibility exhibit a temperature independent Pauli paramagnetic behavior. There is no indication of magnetic ordering, in contrast to the ferrimagnetic behavior associated with the superexchange between Cu(II) and Cr(III) in $\text{CaCu}_3\text{Cr}_2\text{Sb}_2\text{O}_{12}$. Although itinerant electron behavior is similar to that observed for the isostructural $\text{CaCu}_3\text{Ga}_2\text{Ru}_2\text{O}_{12}$, Cu(II)–O–Ru(V) \leftrightarrow Cu(III)–O–Ru(IV) charge transfer is not expected. Rather, a delocalization mechanism involving both CrO_6 and RuO_6 octahedral sublattices is proposed, as is typical for double perovskites. The pure paramagnetic behaviors of $\text{CaCu}_3\text{Ga}_2\text{B}'_2\text{O}_{12}$ ($\text{B}' = \text{Nb, Sb, and Ta}$) perovskites, which contrast with the antiferromagnetic $\text{CaCu}_3\text{Ti}_4\text{O}_{12}$, indicate that the electronic coupling within the A sublattice is strongly influenced by the electronic structure of the B sublattice.

Introduction

Since the first reports of $\text{ACu}_3\text{Ti}_4\text{O}_{12}$ oxides,¹ many members of $\text{AA}'_3\text{B}_4\text{O}_{12}$ ($\text{A} = \text{alkali metals, alkaline earths, lanthanides}$; $\text{A}' = \text{Cu, Mn}$; $\text{B} = \text{Ti, Cr, Mn, Ge, Ru}$) and related families have been reported.^{2–5} This family of compounds shows a distinctive ordering between the 12-coordinated A cations and the 4-coordinated A' cations in the perovskite structure. An unusual square planar coordination for the A' cations is induced by tilts of the BO_6 octahedra, described as $a^+a^+a^+$ using Glazer's nomenclature for octahedral tilt distortions in perovskites.^{4,6} In particular, $\text{ACu}_3\text{B}_4\text{O}_{12}$ perovskites favor this tilting system because the small Jahn–Teller Cu^{2+} cations can fully occupy square planar sites. An interesting and unexpected property, the giant dielectric effect, has been found for one member of the family, $\text{CaCu}_3\text{Ti}_4\text{O}_{12}$.^{7,8} Large magnetoresistance for CaCu_3 -

Mn_4O_{12} and $\text{LaCu}_3\text{Mn}_4\text{O}_{12}$ is another interesting property of $\text{ACu}_3\text{B}_4\text{O}_{12}$ perovskites.^{9,10} This family includes also the metallic $\text{ACu}_3\text{Ru}_4\text{O}_{12}$ ($\text{A} = \text{Na, Ca, Ln}$)¹¹ and $\text{CaCu}_3\text{Cr}_4\text{O}_{12}$.¹²

It is well-known that the physical properties of $\text{A}_2\text{BB}'\text{O}_6$ or $\text{AA}'\text{BB}'\text{O}_6$ perovskites are very sensitive to the nature (i.e., size, electronegativity, electronic configuration) of B and/or B' cations and their arrangements over the octahedral sites.¹³ In contrast, until recently no ordered $\text{AA}'_3\text{B}_2\text{B}'_2\text{O}_{12}$ -type perovskites were known. Therefore, we have recently explored the synthesis of $\text{CaCu}_3\text{Ga}_2\text{B}'_2\text{O}_{12}$ ($\text{B} = \text{Nb, Sb, and Ta}$) at high-pressure high-temperature (HPHT) conditions to provide structural insight into this complex perovskite system.¹⁴ Those materials represented the first examples in which both A site cation order and rock-salt B site order have been observed simultaneously in an $a^+a^+a^+$ perovskite. Subsequently, $\text{CaCu}_3\text{Ga}_2\text{Ru}_2\text{O}_{12}$ and $\text{CaCu}_3\text{Cr}_2\text{Sb}_2\text{O}_{12}$ have also been successfully synthesized at similar high-pressure conditions. Interestingly, $\text{CaCu}_3\text{Ga}_2\text{Ru}_2\text{O}_{12}$, where Ga and Ru cations are disordered over the octahedral sites, shows

* To whom correspondence should be addressed. E-mail: shbyun@khu.ac.kr (S.-H.B.), john.parise@sunysb.edu (J.B.P.).

† Kyung Hee University.

‡ State University of New York.

§ The Ohio State University.

- (1) Deschanvres, A.; Raveau, B.; Tollemer, F. *Bull. Soc. Chim. Fr.* **1967**, 4077.
- (2) Bochu, B.; Chenavas, J.; Jubert, J. C.; Marezio, M. *J. Solid State Chem.* **1974**, *11*, 83.
- (3) Meyer, C.; Gros, Y.; Bochu, B.; Collomb, A.; Chenavas, J.; Jubert, J. C.; Marezio, M. *Phys. Status Solidi, A* **1978**, *48*, 581.
- (4) Bochu, B.; Deschizeaux, M. N.; Jubert, J. C.; Collomb, A.; Chenavas, J.; Marezio, M. *J. Solid State Chem.* **1979**, *29*, 291.
- (5) Labeau, M.; Bochu, B.; Jubert, J. C.; Chenavas, J. *J. Solid State Chem.* **1980**, *33*, 257.
- (6) Glazer, A. M. *Acta Crystallogr., Sect. B* **1972**, *28*, 3384.
- (7) Subramanian, M. A.; Li, Dong; Duan, N.; Reisner, B. A.; Sleight, A. W. *J. Solid State Chem.* **2000**, *151*, 323.
- (8) Homes, C. C.; Vogt, T.; Shapiro, S. M.; Wakimoto, S.; Ramirez, A. P. *Science* **2001**, *293*, 673.

(9) Zeng, Z.; Greenblatt, M.; Subramanian, M. A.; Croft, M. *Phys. Rev. Lett.* **1999**, *82*, 3164.

(10) Alonso, J. A.; Sanchez-Benitez, J.; De Andres, A.; Martinez-Lope, M. J.; Casais, M. T.; Martinez, J. L. *Appl. Phys. Lett.* **2003**, *83*, 2623.

(11) Labeau, M.; Bochu, B.; Joubert, J. C.; Chenavas, J. *J. Solid State Chem.* **1980**, *33*, 257.

(12) Subramanian, M. A.; Marshall, W. J.; Calvarese, T. G.; Sleight, A. W. *J. Phys. Chem. Solids* **2003**, *64*, 1569.

(13) Bonnenberg, D.; Boyd, E. L.; Calhoun, B. A.; Folen, V. J.; Gräper, W.; Greifer, A. P.; Kriessman, C. J.; Lefever, R. A.; McGuire, T. R.; Paulus, M.; Stauss, G. H.; Vautier, R.; Wijn, H. P. J. In *Landolt-Börnstein: Numerical Data and Functional Relationships in Science and Technology*; Hellwege, K. H., Ed.; New Series, Group III; Springer-Verlag: Berlin, 1970; Vol. 4b.

(14) Byeon, S.-H.; Lufaso, M. W.; Parise, J. B.; Woodward, P. M.; Hansen, T. *Chem. Mater.* **2003**, *15*, 3798.

metallic conductivity thought to originate from a valence degeneracy between Cu(II) + Ru(V) and Cu(III) + Ru(IV).¹⁵ CaCu₃Cr₂Sb₂O₁₂ showing simultaneous cation ordering on both A and B sites is a ferrimagnet, the spontaneous magnetization being associated with the Cu(II)–Cr(III) superexchange interaction.¹⁶

The localized or collective electronic property observed in those compounds, which is dependent on the nature of the B sublattice, is quite similar to those in A₂BB'O₆ or AA'BB'O₆ perovskites. The attractiveness of studying the AA'B₂B'O₁₂ system comes from the competing interaction between A and B sublattices because of unusual stabilization of dⁿ transition metal cations in the A sites. To establish the general description of such a complex interaction, it is necessary to synthesize and characterize many more members of the AA'B₂B'O₁₂ perovskite family. In this study we have synthesized and characterized CaCu₃Cr₂Ru₂O₁₂, which can be added to the list of CaCu₃B₂B'O₁₂ perovskites. To the best of our knowledge, this combination is the first example for the Cr/Ru pair stabilized in the B sites of a perovskite-type oxide.

Experimental Section

CaCu₃Cr₂Ru₂O₁₂ was synthesized by the solid-state reaction accompanied by HPHT treatment. An appropriate stoichiometric mixture of dried CaCO₃, CuO, Cr₂O₃, and RuO₂ was calcined at 850 °C in air for 10 h with intermittent grinding. The reacted oxide mix was then thoroughly reground and sealed in a Au capsule with an inside diameter of 3.2 mm and a wall thickness of 0.1 mm. The sample was then subjected to HPHT conditions at 12 GPa and 1150 °C, followed by temperature quenching and slow decompression using the 2000-ton Uniaxial Split Sphere high-pressure apparatus (USSA 2000).¹⁷ The sample was recovered from the Au capsule as a dense pellet with an approximate volume of 50 mm³.

The formation of a perovskite-related phase was initially confirmed from an X-ray diffraction pattern, taken on the sample pellet after recovery from the HPHT reaction using a general area detector diffraction system (GADDS). All major peaks in the powder diffraction pattern could be indexed on the basis of a body-centered cubic cell with an approximate cell dimension $a \sim 7.40$ Å. Intensity data suitable for Rietveld structure refinement were collected from a MacScience model M18XHF diffractometer installed on a rotating anode X-ray source operating at 40 kV and 300 mA. Monochromatic Cu K α radiation was obtained using a curved-crystal of graphite. The data were collected with a step-scan procedure in the range $2\theta = 10\text{--}120^\circ$ with a step width of 0.02° and a step time of 1 s. The unit cell parameter was derived by least-squares refinement using the peak positions obtained from the powder diffraction data. Because of the limited quantity of sample recovered after the high-pressure treatment, the diffraction intensity data were obtained for a small amount of powder sample dispersed on a glass plate with absolute ethanol. The refinement of structural and instrumental parameters was carried out using the Rietveld analysis program RIETAN-2000.¹⁸

Elemental analysis using the energy-dispersive X-ray (EDX) emission technique gave the stoichiometric composition within experimental errors. Direct current magnetic susceptibility measurement for the sample powder was carried out in the temperature range from 5 to 300 K in an applied magnetic field of 0.5 T using a Quantum Design MPMS-5 SQUID magnetometer. Isothermal magnetization curves were recorded up to 5 T after cooling the sample in zero magnetic field to 10 K. Electrical resistivity was measured using a standard four-probe technique on the polycrystalline sample obtained directly as a dense pellet from the high-pressure synthesis. Data were collected in the temperature range 10–300 K in a closed-cycle helium cryostat.

Results and Discussion

The software program SPuDS (Structure Prediction Diagnostic Software) was useful to calculate ideal structures of perovskites by optimizing the bond valence sums of the ions in the crystal structure.¹⁹ The minimized global instability index (GII) is an indication of the composition stability, with a lower value indicating a more stable structure. As part of a program designed to develop new members of the CaCu₃B₂B'O₁₂ perovskite family, many compositions were predicted by SPuDS to be stable under HPHT conditions. Among them, the composition CaCu₃Cr₂Ru₂O₁₂ produced a sufficiently small GII value (~ 0.007) and was selected as a target of our synthetic efforts. Comparison with prior results suggests that there should be an interesting competition between electron delocalization and magnetically ordered localized electrons in this compound. On one hand, strong charge hybridization between Cu(II) and Ru(V) cations leading to metallic conductivity might be expected as observed in CaCu₃Ga₂Ru₂O₁₂.¹⁵ On the other hand, relatively strong superexchange interactions between Cu(II) and Cr(III) cations leading to ferrimagnetic behavior might be expected as observed in CaCu₃Cr₂Sb₂O₁₂.¹⁶ It should be noted that both charge transfer and superexchange were attributed to an interaction between A and B sublattices of the perovskite structure.

Attempts to synthesize a perovskite with composition CaCu₃Cr₂Ru₂O₁₂ at ambient pressure by reacting oxide mixes in air and O₂ flowing for a long period ($t > 50$ h) were not successful. Although a cubic phase that is considered as the target compound CaCu₃Cr₂Ru₂O₁₂ was obtained at ambient pressure, significant CaCrO₄ and CuCrO₂ were observed below 850 °C and CaCrO₃ impurity was observed at 950 °C. The initial X-ray powder diffraction pattern collected on a GADDS showed that CaCu₃Cr₂Ru₂O₁₂ was isolated as the dominant phase after temperature quenching of the sample reacted at high-pressure conditions for 1 h.

The CaCu₃Ti₄O₁₂ phase is well-known to crystallize in the perovskite-related structure with space group $Im\bar{3}$ with strong tilting of TiO₆ octahedra.² Replacement of Ti by two different cations B and B' with an equal ratio on the octahedral site leads to the possibility of the same tilt system with ordered arrangement of cations. Ordering of octahedral cations in the $a^+a^+a^+$ tilt system changes the space group symmetry

(15) Byeon, S.-H.; Lee, S.-S.; Parise, J. B.; Woodward, P. M.; Hur, N. H. *Chem. Mater.* **2004**, *16*, 3697.

(16) Byeon, S.-H.; Lee, S.-S.; Parise, J. B.; Woodward, P. M.; Hur, N. H. *Chem. Mater.* **2005**, *17*, 3552.

(17) Liebermann, R. C.; Wang, Y. *High-Pressure Research: Application to Earth and Planetary Sciences*; Terrapub: Tokyo, 1992.

(18) Izumi, F.; Murata, H.; Watanabe, N. *J. Appl. Crystallogr.* **1987**, *20*, 411.

(19) Lufaso, M. W.; Woodward, P. M. *Acta Crystallogr., Sect. B* **2001**, *57*, 725.

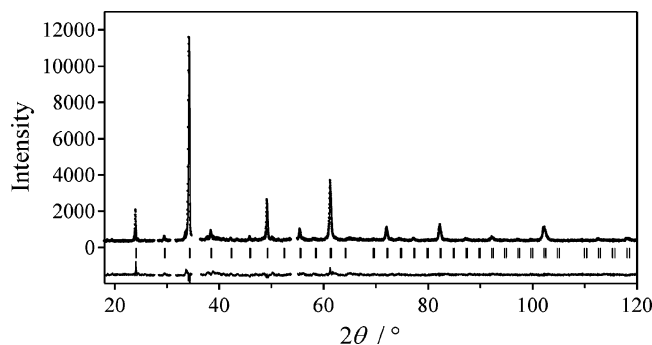


Figure 1. Observed X-ray powder diffraction data (dotted line) along with the calculated diffraction pattern (solid line) obtained from Rietveld refinement of $\text{CaCu}_3\text{Cr}_2\text{Ru}_2\text{O}_{12}$. Regions of the pattern containing impurity peaks are excluded. At the bottom of the figure the difference plot ($I_{\text{obs}} - I_{\text{calc}}$) is shown on the same scale. Vertical bars on the bottom indicate the positions of allowed Bragg reflections.

from $Im\bar{3}$ to $Pn\bar{3}$.²⁰ The characteristic (111) peak, with an intensity sensitive to the degree of B site ordering, appears in the X-ray diffraction pattern for this ordered perovskite structure. However, the X-ray powder diffraction pattern of $\text{CaCu}_3\text{Cr}_2\text{Ru}_2\text{O}_{12}$ showed no intensity at the angle expected for the (111) reflection, as was previously obtained for $\text{CaCu}_3\text{Ga}_2\text{Ru}_2\text{O}_{12}$.¹⁵ This comparison implied that $\text{CaCu}_3\text{Cr}_2\text{Ru}_2\text{O}_{12}$ crystallizes in space group $Im\bar{3}$ with Cr and Ru randomly distributed over the available octahedral sites. Accordingly, the atomic positions of disordered perovskite $\text{CaCu}_3\text{Ga}_2\text{Ru}_2\text{O}_{12}$ were used in the initial stages of structure refinement. Some peaks attributed to impurities ($I/I_{\text{max}} < 0.05$) were present in repeated reactions carried out at different temperature and pressure conditions. The positions of these peaks corresponded neither to X-ray patterns obtained after ambient pressure heat treatments (i.e., CaCrO_4 , CaCrO_3 , and/or CuCrO_2) nor to those expected for likely minority phases, such as CuO , Cr_2O_3 , CrO_2 , RuO_2 , and CaRuO_3 . Multiple attempts to identify the impurity phase(s) were unsuccessful largely because of their low intensities, and these trace impurities may also correspond to pressure stabilized phases. When the regions corresponding to the strongest peaks from the impurity phase(s) were thus excluded from subsequent Rietveld refinement, the residual fit parameter was noticeably reduced.

The observed diffraction data as well as the calculated pattern and difference curve from the Rietveld refinement of $\text{CaCu}_3\text{Cr}_2\text{Ru}_2\text{O}_{12}$ are shown in Figure 1. Crystallographic data, including refined atomic coordinates and isotropic displacement parameters, are listed in Table 1. As shown in Figure 2, $\text{CaCu}_3\text{Cr}_2\text{Ru}_2\text{O}_{12}$ is isostructural with $\text{CaCu}_3\text{B}_4\text{O}_{12}$ ⁴ because of a statistical distribution of Cr and Ru in the B sites. Selected interatomic distances and angles are compared to those of other members of this family of structures as shown in Table 2. Copper is at the center of a slightly distorted square planar site with O—Cu—O angles deviating only slightly from 90°. The O—(Cr/Ru)—O angles close to 90° are consistent with the tilting of essentially rigid octahedra. In general the Cu—O distance and (Cr/Ru)—O—(Cr/Ru) angles are very similar to those previously obtained

Table 1. Structure Refinement Results for $\text{CaCu}_3\text{Cr}_2\text{Ru}_2\text{O}_{12}$

compound	$\text{CaCu}_3\text{Cr}_2\text{Ru}_2\text{O}_{12}$			
R_{wp} (%)	8.01			
R_{p} (%)	5.92			
R_{E} (%)	4.55			
R_{F} (%)	8.08			
space group	$Im\bar{3}$			
a (Å)	7.4100(8)			
Atomic Positions ^{a,b}				
atom	x	y	z	U_{iso} (Å ²)
Ca	0.0	0.0	0.0	0.027(2)
Cu	0.0	0.5	0.5	0.039(1)
Cr/Ru	0.25	0.25	0.25	0.0061(5)
O	0.0	0.181(1)	0.307(1)	0.009(2)

^a $Im\bar{3}$, Ca(2a), Cu(6b), Cr/Ru(8c), O(24g) ^b The site occupancies of all atoms were fixed to 1.0.

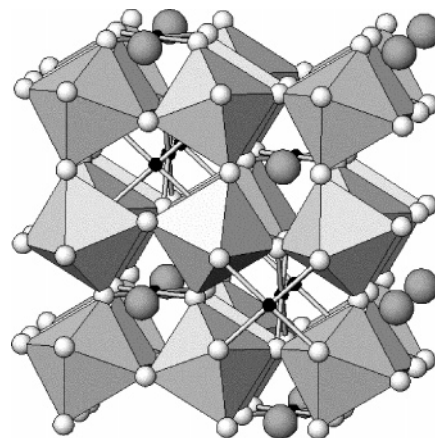


Figure 2. Idealized structure of $\text{CaCu}_3\text{Cr}_2\text{Ru}_2\text{O}_{12}$. Cr and Ru are statistically distributed over octahedral sites. Large spheres and small black spheres represent Ca and Cu atoms, respectively. Cu—O bonds in the 4-coordinated CuO_4 arrangement are represented.

for other $\text{CaCu}_3\text{B}_4\text{O}_{12}$ compounds. However, the B/B' = Ga/Ru member exhibits a significantly shorter Cu—O distance and smaller (Ga/Ru)—O—(Ga/Ru) angles. Such a difference suggests it would be instructive to compare the transport properties of $\text{CaCu}_3\text{Cr}_2\text{Ru}_2\text{O}_{12}$ with those of $\text{CaCu}_3\text{Ga}_2\text{Ru}_2\text{O}_{12}$.

Figure 3a shows the temperature-dependent electrical resistivity data of $\text{CaCu}_3\text{Cr}_2\text{Ru}_2\text{O}_{12}$. The behavior is clearly consistent with metallic behavior. The electrical conductivity is higher than that of $\text{CaCu}_3\text{Ga}_2\text{Ru}_2\text{O}_{12}$ (Figure 3b). Considering the significantly shorter Cu—O distance and strong distortion of the (Ga/Ru)—O—(Ga/Ru) angle, the metallic property of $\text{CaCu}_3\text{Ga}_2\text{Ru}_2\text{O}_{12}$ was attributed to Cu(II)—O—Ru(V) \leftrightarrow Cu(III)—O—Ru(IV) charge transfer.¹⁵ An unusually high bond valence sum (2.31) for Cu also supported a significant oxidation of Cu(II) by Ru(V). In Table 3, we compare the bond valence sums of members of the $\text{CaCu}_3\text{B}_2\text{B}'_2\text{O}_{12}$ family, calculated using $\nu_{ij} = \exp[(R_{ij} - d_{ij})/b]$ where R_{ij} and d_{ij} are the bond valence parameter and bond length, respectively, and b is a universal constant equal to 0.37.²¹ Replacement of Ga by Cr in $\text{CaCu}_3\text{Ga}_2\text{Sb}_2\text{O}_{12}$ gives no noticeable change in the oxidation state of Cu whereas the same replacement in $\text{CaCu}_3\text{Ga}_2\text{Ru}_2\text{O}_{12}$ considerably

(20) Howard, C. J.; Kennedy, B. J.; Woodward, P. M. *Acta Crystallogr., Sect. B* **2003**, *59*, 463.

(21) Brown, I. D. *The Chemical Bond in Inorganic Chemistry. The Bond Valence Model*; IUCr Monograph on Crystallography; Oxford University Press: Oxford, 2002; Vol. 12.

Table 2. Comparison of Selected Bond Lengths and Bond Angles for $\text{CaCu}_3\text{B}_2\text{B}'_2\text{O}_{12}$

B/B'	Cr/Ru	Ga/Ru ¹⁵	Cr/Sb ¹⁶	Ga/Nb ¹⁴	Ga/Sb ¹⁴	Ga/Ta ¹⁴
Bond Distances (Å)						
Ca–O (×12)	2.639(8)	2.609(4)	2.585(8)	2.66(1)	2.6274(7)	2.6323(8)
Cu–O (×4)	1.964(6)	1.895(3)	1.973(7)	1.96(1)	1.9691(6)	1.9764(7)
B–O (×6)	1.966(4) ^a	2.002(4) ^a	1.926(6)	1.989(4) ^a	1.999(2)	1.981(6)
B'–O (×6)			2.048(6)		1.961(1)	1.986(6)
Bond Angles (deg)						
O–Cu–O (×2)	86.3(8)	82.5(8)	82.0(7)	86.0(4)	84.65(4)	84.61(5)
O–Cu–O (×2)	93.7(8)	97.5(8)	98.0(7)	94.0(4)	95.36(4)	95.39(5)
O–B–O (×6)	89.3(6) ^b	89.1(6) ^b	88.0(5)	89.3(4) ^b	89.61(3)	89.59(3)
O–B'–O (×6)			87.9(5)		89.68(3)	89.59(3)
O–B–O (×6)	90.7(6) ^b	90.9(6) ^b	92.0(5)	90.7(4) ^b	90.39(3)	90.41(3)
O–B'–O (×6)			92.1(5)		90.32(3)	90.41(3)
B–O–B'	140.8(3) ^c	136.2(6) ^c	139.5(4)	139.7(5) ^c	140.26(3)	140.40(4)

^a B/B'–O average distance. ^b O–B/B'–O angle. ^c B/B'–O–B/B' angle.

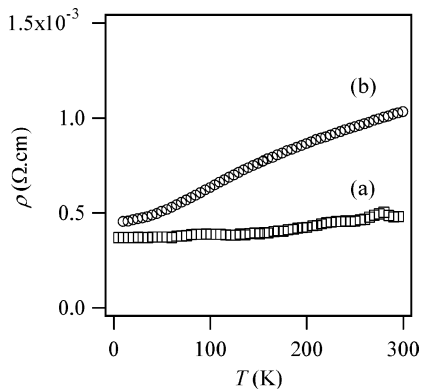


Figure 3. Plots of resistivity versus temperature for (a) $\text{CaCu}_3\text{Cr}_2\text{Ru}_2\text{O}_{12}$ and (b) $\text{CaCu}_3\text{Ga}_2\text{Ru}_2\text{O}_{12}$.

Table 3. Bond Valence Sums of the Ions in $\text{CaCu}_3\text{B}_2\text{B}'_2\text{O}_{12}$

B/B'	Cr/Ru	Ga/Ru	Cr/Sb	Ga/Nb	Ga/Sb	Ga/Ta
Ca	1.95	2.12	2.26	1.85	2.01	1.99
Cu	2.06	2.31	2.05	2.06	2.07	2.03
B			3.24		2.90	3.04
B'			4.80		5.70	5.02

reduces the bond valence sum for Cu from 2.31 to 2.06. Thus, we speculate that the metallic behavior observed in $\text{CaCu}_3\text{Cr}_2\text{Ru}_2\text{O}_{12}$ is largely associated with an itinerant (Cr/Ru)–O–(Cr/Ru) interaction rather than a valence degeneracy between Cu(II) + Ru(V) and Cu(III) + Ru(IV) combinations. However, it should be noted that many other double perovskite oxides such as $\text{La}_2\text{CrMnO}_6$,²² $\text{Sr}_2\text{FeRuO}_6$,²³ BaLaNiRuO_6 ,²³ LaSrCoRuO_6 ,²⁴ $\text{Sr}_2\text{CoRuO}_6$,²⁵ and SrLaCuRuO_6 ²⁶ with a transition metal/Cr or Ru pair in the B/B' sites reveal the localized electronic property despite much larger B/B'–O–B/B' bond angles ($>150^\circ$). Because the (Cr/Ru)–O–(Cr/Ru) angle is important for Ru 4d–O 2p and Cr 3d–O 2p orbital overlaps, an explanation for the collective electronic behavior of $\text{CaCu}_3\text{Cr}_2\text{Ru}_2\text{O}_{12}$ is not straightforward. Considering that $\text{CaCu}_3\text{Cr}_4\text{O}_{12}$ and $\text{CaCu}_3\text{Ru}_4\text{O}_{12}$ are metallic,^{12,27} Cr(III)–O–Ru(V) \leftrightarrow Cr(IV)–O–Ru(IV) charge transfer in the B sublattice could be introduced to describe

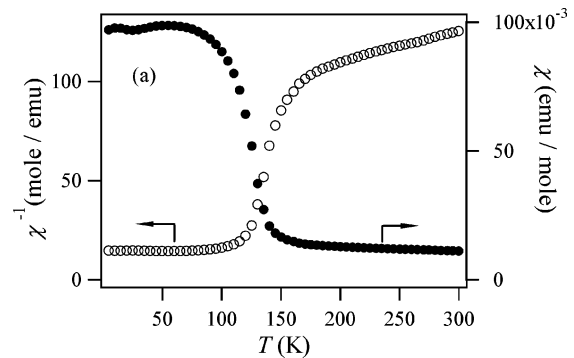


Figure 4. Temperature dependence of the molar magnetic susceptibility measured at 0.5 T.

this itinerant behavior. Another interesting feature of these compounds is that they are Pauli paramagnetic, which implies that Cu 3d states are at least partially involved in the electronic structure near the Fermi level. It seems likely that Cu 3d states could also play an important role in the electron delocalization seen in $\text{CaCu}_3\text{Cr}_2\text{Ru}_2\text{O}_{12}$.

Magnetic susceptibility of $\text{CaCu}_3\text{Cr}_2\text{Ru}_2\text{O}_{12}$ as a function of temperature (Figure 4) exhibits a temperature independent Pauli paramagnetic behavior at $T > 140$ K, consistent with itinerant electron behavior. Because the magnetic susceptibility showed a broad shoulder below 140 K, however, the field dependence of magnetization for $\text{CaCu}_3\text{Cr}_2\text{Ru}_2\text{O}_{12}$ was measured. A small hysteresis was present at 10 K, and the remnant magnetization corresponded to $\sim 0.05 \mu_B$ per formula unit. This value is not comparable with 15 or 9 μ_B /f.u. expected for parallel alignment of all magnetic moments or antiparallel alignment of Cu(II) and Cr(III)/Ru(V) spins, respectively. Concerning an interaction between Cr(III) and Ru(V) in the B sublattice, the magnetic exchange between d^3 electronic configuration is expected to be antiferromagnetic rather than ferromagnetic according to the superexchange rule.¹³ All considerations suggest that the weak remnant magnetization at low temperature is due to a small ferromagnetic impurity which is not distinguished in the X-ray diffraction pattern.

A replacement of Sb by Ru in $\text{CaCu}_3\text{Cr}_2\text{Sb}_2\text{O}_{12}$ results in essentially complete disruption of the magnetic interaction between the A site Cu(II) and the B site Cr(III) cations, indicating that the change of arrangement manner in the B sublattice completely alters the superexchange mechanisms in the whole lattice. As compared in Figure 5, the observed

(22) Tanaka, H.; Okawa, N.; Kawai, T. *Solid State Commun.* **1999**, *110*, 191.

(23) Battle, P. D.; Gibb, T. C.; Jones, C. W.; Studer, F. J. *Solid State Chem.* **1989**, *78*, 281.

(24) Bos, J. W. G.; Atfield, J. P. *Chem. Mater.* **2004**, *16*, 1822.

(25) Kim, S. H.; Battle, P. D. *J. Solid State Chem.* **1995**, *114*, 174.

(26) Fernandez, I.; Greatrex, R.; Greenwood, N. N. *J. Solid State Chem.* **1980**, *32*, 97.

(27) Subramanian, M. A.; Sleight, A. W. *Solid State Sci.* **2002**, *4*, 347.

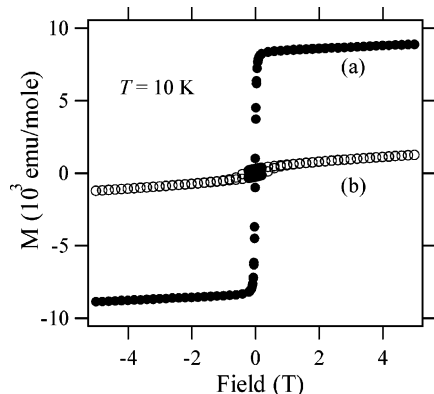


Figure 5. Comparison of magnetization loops for (a) $\text{CaCu}_3\text{Cr}_2\text{Sb}_2\text{O}_{12}$ and (b) $\text{CaCu}_3\text{Cr}_2\text{Ru}_2\text{O}_{12}$ at 10 K.

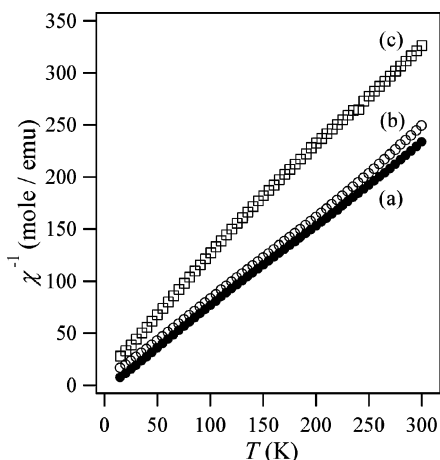


Figure 6. Plots of inverse molar magnetic susceptibility versus temperature for (a) $\text{CaCu}_3\text{Ga}_2\text{Sb}_2\text{O}_{12}$, (b) $\text{CaCu}_3\text{Ga}_2\text{Ta}_2\text{O}_{12}$, and (c) $\text{CaCu}_3\text{Ga}_2\text{Nb}_2\text{O}_{12}$.

magnetization of $\sim 1.4 \mu_B$ for $\text{CaCu}_3\text{Cr}_2\text{Sb}_2\text{O}_{12}$ was attributed to a significant canting of antiparallel alignment of Cu(II) and Cr(III) spins.¹⁶ Furthermore, no ferromagnetism was observed in the $\text{CaCu}_3\text{B}_2\text{B}'_2\text{O}_{12}$ analogues where both the B and the B' are nonmagnetic cations, and the possible superexchange between A site Cu(II) cations is antiferromagnetic. For instance, $\text{CaCu}_3\text{Ti}_4\text{O}_{12}$ shows an antiferromagnetic order below 27 K, resulting from superexchange between (111) Cu–O planes.²⁸ For a more general comparison, we plotted the inverse magnetic susceptibility data of $\text{CaCu}_3\text{Ga}_2\text{B}'_2\text{O}_{12}$ ($\text{B}' = \text{Nb}, \text{Sb}, \text{and Ta}$) as a function of temperature in Figure 6. No magnetic ordering is observed with these compounds in the measured temperature range

(5–300 K). Instead, the magnetic properties of these members show a pure paramagnetic behavior and obey a Curie–Weiss law. Observed effective magnetic moments of 1.69, 1.74, and $1.76 \mu_B/\text{Cu}$ for $\text{CaCu}_3\text{Ga}_2\text{Nb}_2\text{O}_{12}$, $\text{CaCu}_3\text{Ga}_2\text{Sb}_2\text{O}_{12}$, and $\text{CaCu}_3\text{Ga}_2\text{Ta}_2\text{O}_{12}$, respectively, are in good agreement with the theoretical spin-only value of $1.73 \mu_B$ for Cu(II). Considering the unit cell dimension ($a = 7.391 \text{ \AA}$) of $\text{CaCu}_3\text{Ti}_4\text{O}_{12}$, relatively long distance interplane (111) magnetic superexchange beyond the TiO_6 octahedral sublattice would be significantly weakened in the expanded lattices ($a = 7.44\text{--}7.47 \text{ \AA}$) of these compounds. More importantly, a difference in structural and electronic environment of the B sublattice could be a crucial factor to reduce the magnetic interactions in the A sublattice. Consequently, the temperature independent paramagnetic behavior of $\text{CaCu}_3\text{Cr}_2\text{Ru}_2\text{O}_{12}$, coupled with the calculated bond valence sum of Cu, indicates that a delocalization mechanism involving both the CrO_6 and the RuO_6 octahedral sublattice is predominant over an influence of A site Cu(II). This behavior is in contrast to the strong correlation between the A and the B sublattices which is observed in other members such as $\text{CaCu}_3\text{Ga}_2\text{Ru}_2\text{O}_{12}$ and $\text{CaCu}_3\text{Cr}_2\text{Sb}_2\text{O}_{12}$.

Conclusions

Despite many members of the family of perovskite ruthenates with general formula A_2BRuO_6 , $\text{AA}'\text{BRuO}_6$, and $\text{A}_3\text{BRu}_2\text{O}_9$, no example has been reported for the Cr/Ru pair stabilized in the B/B' sites of a perovskite-type oxide. In this study, $\text{CaCu}_3\text{Cr}_2\text{Ru}_2\text{O}_{12}$ has been explored, successfully synthesized under conditions of HPHT, and recovered to room pressure conditions. The Cr and Ru atoms in the perovskite-like structure are disordered over the octahedral sites. Magnetic susceptibility and electrical transport measurement data show that this oxide is a Pauli paramagnetic conductor. Comparison with the metallic $\text{CaCu}_3\text{Ga}_2\text{Ru}_2\text{O}_{12}$ and the ferrimagnetic $\text{CaCu}_3\text{Cr}_2\text{Sb}_2\text{O}_{12}$ suggests that no $\text{Cu(II)}\text{--O--Ru(V)} \leftrightarrow \text{Cu(III)}\text{--O--Ru(IV)}$ charge transfer and no superexchange between Cu(II) and Cr(III) occur. This leads us to conclude that an explanation of the localized or itinerant electronic behaviors induced in the $\text{CaCu}_3\text{B}_2\text{B}'_2\text{O}_{12}$ family should include the interactions in the A and B sublattices as well as between the A and the B sublattices.

Acknowledgment. J.B.P. acknowledges the support of NSF through its DMR (04524444) and EAR (0510501) programs. Research carried out at Kyung Hee University was supported by Korea Research Foundation Grant (KRF-2004-041-C00189).

(28) Collomb, A.; Samaras, D.; Bochu, B.; Joubert, J. C. *Phys. Status Solidi, A* **1977**, *41*, 459.